JCTC Journal of Chemical Theory and Computation

ARTICLE

pubs.acs.org/JCTC

Validation of the GROMOS 54A7 Force Field with Respect to β-Peptide Folding

Wei Huang, Zhixiong Lin, and Wilfred F. van Gunsteren*

Laboratory of Physical Chemistry, Swiss Federal Institute of Technology, ETH, 8093 Zürich, Switzerland

ABSTRACT: The recently developed GROMOS 54A7 force field, a modification of the 53A6 force field, is validated by simulating the folding equilibrium of two β-peptides which show different dominant folds, i.e., a 3_{14}-helix and a hairpin, using three different force fields, i.e., GROMOS 45A3, 53A6, and 54A7. The 54A7 force field stabilizes both folds, and the agreement of the simulated NOE atom−atom distances with the experimental NMR data is slightly improved when using the 54A7 force field, while the agreement of the ^3J couplings with experimental results remains essentially unchanged when varying the force field. The 54A7 force field developed to improve the stability of α-helical structures in proteins can thus be safely used in simulations of β-peptides.

1. INTRODUCTION

Molecular dynamics simulation is an efficient method used to understand and predict biological or chemical processes at the atomic level. The simulation results, however, depend on the quality of the force field used, which describes the interactions between particles in the system. Several force fields have been developed for biomolecular simulation, such as AMBER,[1−3] CHARMM,[4−6] GROMOS,[7−11] and OPLS.[12,13] Over the years, successive GROMOS force-field parameter sets have been introduced.[9−11] The most widely used versions of this force field are the 43A1 force field[8,9] of 1996, the 45A3 force field[10] of 2001, and the 53A6 force field[11] of 2004.

The force field 43A1 contains 43 individual atom types to describe van der Waals interactions.[9] The force field 45A3 introduced two additional atom types for branched and cyclic alkanes and reparameterized the aliphatic CH_n groups based on thermodynamic data for long alkane chains.[10] The force field 53A6 reparameterized a number of polar groups also against thermodynamic data, including several (co)solvents,[14−17] renumbered all atom, bond, bond−angle, and torsional dihedral-angel types, and added eight new van der Waals atom types. The recently developed force field 54A7[18] is a modification of the 53A6 force field. It contains four modifications: (1) The torsional angle energy term for the polypeptide φ- and ψ-dihedral angles is modified. Four different torsional dihedral angle types are added, and the repulsive van de Waals $C_{12}^{1/2}$(I, I) parameter for the O−N pair is changed to be smaller than that in the 53A6 parameter set. (2) A new van der Waals nonbonded atom type for a charged $-CH_3$ group is introduced in order to generate a larger repulsion between the partly charged $-CH_3$ groups of the choline moiety and the negatively charged OM oxygen atoms of the phosphate moiety in DPPC type lipids.[19] (3) The van der Waals nonbonded interaction parameters for the Na^+ and Cl^- ions are changed. (4) Two additional improper dihedral angle types are defined in order to facilitate free energy difference calculations involving chirality changes. The first modification was introduced[18] in order to redress the tendency of the thermodynamically calibrated 53A6 force field to slightly destabilize α-helical structures in proteins. Application to four different proteins shows that the new 54A7 force field has the intended effect.[18] However, a more stringent test than simulating folded proteins would be the simulation of a folding equilibrium, which is only possible for short polypeptides.

β-Peptides are non-natural polypeptides which exhibit a strong tendency to form stable, well-defined secondary structures.[20−22] Their resistance to degradation by proteases makes them attractive as potential pharmaceuticals.[23,24] β-Peptides can form stable secondary structure motifs even at much shorter sequence lengths than those needed in α-peptides.[25,26] This feature makes them ideal cases to study the folding process and test the quality of the force field in molecular dynamics simulations[27−29] of the folding equilibrium. Since the modification of the peptidic φ- and ψ-angle torsional angle energy terms and the change in $C_{12}^{1/2}$(I, I) repulsive van der Waals parameters for backbone N−O atom pairs would influence the folding equilibrium of β-peptides, a test of the 54A7 force field with respect to its reproduction of β-peptide folding is necessary.

Here, we test the new GROMOS force field parameter set 54A7 with respect to β-peptide folding using two β-peptides which in methanol fold into different secondary structures: peptide **1**,[30−32] whose dominant fold is a 3_{14}-helix, and peptide **2**,[33] whose dominant fold is a hairpin (Figure 1). Both β-peptides were previously used to study the effect of the use of a polarizable methanol solvent model on their folding equilibrium.[34] The results of the simulations using the 54A7 parameter set are compared to the results obtained with two earlier parameter sets, 53A6 and 45A3, as well as to the NMR experimental data of these two β-peptides.

2. METHODS

2.1. 54A7 Parameter Set. The torsional angle energy term for the polypeptide φ- and ψ-dihedral angles is modified in conjunction with a change of the combination prescription of the C_{12}

Received: December 24, 2010
Published: April 20, 2011

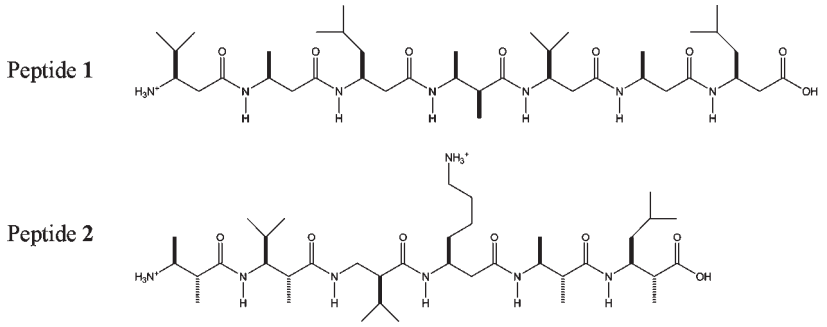

Figure 1. Chemical formulas of the two β-peptides: peptide **1**, H_2^+-β^3-HVal-β^3-HAla-β^3-HLeu-(S,S)-β^3-HAla(αMe)-β^3-HVal-β^3-HAla-β^3-HLeu-OH; Peptide **2**, H_2^+-(S,R)-β^3-HAla(αMe)-(S,R)-β^3-HVal(αMe)-β^2-HVal-β^3-HLys-(S,R)-β^3-HAla(αMe)-(S,R)-β^3-HLeu(αMe)-OH.

Table 1. New Torsional Dihedral Angle Parameters[a] in the GROMOS 54A7 Force Field

type code	K_{ϕ_n} kJ mol^{-1}	cos(δ_n)	m_n	example
42	3.50	−1	2	−CH$_n$−C−
43	2.80	+1	3	−CH$_n$−N−
44	0.70	−1	6	−CH$_n$−N−
45	0.40	+1	6	−CH$_n$−C−

[a] The definition of the parameters can be found in ref 11, Table 5.

van der Waals parameters for the atom type pair O(IAC=1)−N(IAC=6):

(a) In the selection table (Table 8 of ref 11), for the repulsive van der Waals $C_{12}^{1/2}$(I, I) parameters, the type for the O(IAC=1)−N(IAC=6) pair is changed from "2" to "1". This means that the smaller $C_{12}^{1/2}$(O, O) value of 1.000 × 10^{-3} [kJ mol^{-1} nm^{12}]$^{1/2}$ for the O atom (IAC=1) is selected for the interaction with an N atom (IAC=6) compared to the $C_{12}^{1/2}$(O, O) value of 1.130 × 10^{-3} [kJ mol^{-1} nm^{12}]$^{1/2}$ in 53A6.

(b) Four different torsional dihedral angle types are added to Table 5 of ref 11, see Table 1. In the molecular topology building blocks for α-peptides and β-peptides, the dihedral angle type 39 (53A6) in the backbone C−N−CA−C dihedral (α-residue) or the backbone C−N−CB−CA dihedral (β-residue) is to be changed to type 44 (54A7), and the same dihedral angle with type 43 (54A7) is added. In addition, the dihedral angle type 40 (53A6) for the backbone N−CA−C−N dihedral (α-residue) or the backbone CB−CA−C−N dihedral (β-residue) is to be changed into type 45 (54A7), and the same dihedral angle with type 42 (54A7) is added.

These changes increase the hydrogen bonding between the N−H and the C═O groups in the polypeptide backbone and bring the φ- and ψ-angle distributions for a number of proteins more in line[18] with the preferences observed in PDB protein structures.

2.2. Simulations. Six molecular dynamics simulations, of the two β-peptides and based on the 45A3, 53A6, and 54A7 parameter sets, were carried out using the GROMOS05 software,[35] see Table 2. The backbone termini of peptides **1** and **2** and the Lys side chain of peptide **2** were protonated. No counterions were used. The methanol model included in the 45A3 force field is slightly different from the one used in the 53A6 and 54A7 force fields.[11,14] For peptide **1** and parameter set 45A3, a trajectory of a previous simulation was used.[36]

Table 2. Overview of the MD Simulations

peptide	simulation name	force field	charge state [e]	no. solvent molecules
Peptide **1**	$\mathbf{1}_{45A3}$[a]	45A3	+1	1090
	$\mathbf{1}_{53A6}$	53A6	+1	1090
	$\mathbf{1}_{54A7}$	54A7	+1	1096
Peptide **2**	$\mathbf{2}_{45A3}$	45A3	+2	1409
	$\mathbf{2}_{53A6}$	53A6	+2	1366
	$\mathbf{2}_{54A7}$	54A7	+2	1409

[a] The trajectory of this simulation is described in ref 36.

The folded conformations of the two peptides were used as initial structures. Each peptide was solvated in a periodic, rectangular box with methanol as the solvent. The minimum distance from any peptide atom to the box wall was set to 1.4 nm in both cases. The resulting numbers of solvents are listed in Table 2.

Both simulations were carried out for 200 ns at a constant temperature of 340 K and a constant pressure of 1 atm using the weak coupling algorithm.[37] The temperature coupling time was set to 0.1 ps and the pressure coupling time to 0.5 ps, and an isothermal compressibility of 4.575 × 10^{-4} (kJ mol^{-1} nm^{-3})$^{-1}$ was used.[8] All bond lengths were kept rigid at ideal bond lengths using the SHAKE algorithm,[38] as was the H−CH$_3$ distance in methanol, allowing a time step of 2 fs in the leapfrog algorithm to integrate the equations of motion. Nonbonded interactions were calculated using a twin-range cutoff scheme with cutoff radii of 0.8/1.4 nm. Interactions within 0.8 nm were evaluated every time step. The intermediate range interactions were updated every fifth time step, and the long-range electrostatic interactions beyond 1.4 nm were approximated by a reaction field force[39] representing a dielectric continuum with a dielectric permittivity of either 17.7 for the methanol model of the 45A3 force field or 19.8 for that of the 53A6 and 54A7 force fields.[14]

2.3. Analysis. Trajectory coordinates and energies stored at 0.5 ps intervals were used for analysis. Backbone atom-positional root-mean-square deviations (RMSD) were calculated after translational superposition of the solute centers of mass and least-squares rotational fitting of atomic positions, using all backbone atoms (N, CB, CA, C) of residues 2−6 for peptide **1** and residues 2−5 for peptide **2**. The backbone atom-positional RMSD criteria required to separate the folded conformation (C_F) from the unfolded ones (C_U) are 0.1 nm for peptide **1** and

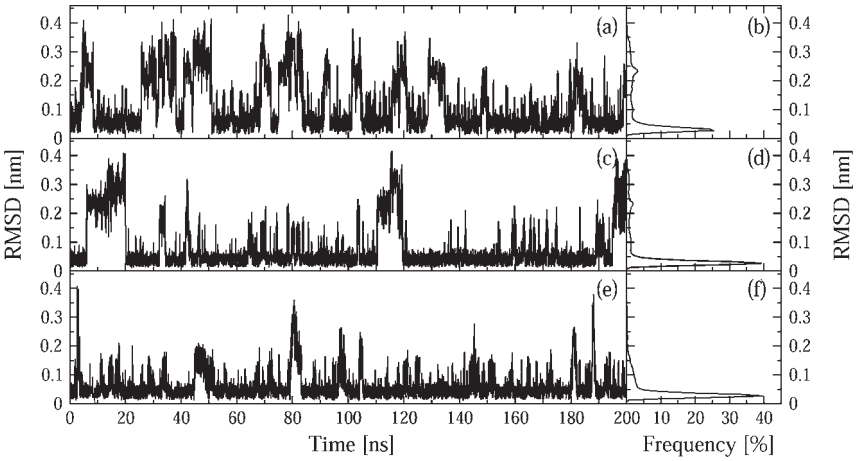

Figure 2. Time evolution (left panels) and distribution (right panels) of atom-positional RMSD from the 3_{14}-helical model structure for the backbone atoms of residues 2−6 in simulations of peptide **1**. Upper panels, $\mathbf{1}_{45A3}$; middle panels, $\mathbf{1}_{53A6}$; lower panels, $\mathbf{1}_{54A7}$.

0.08 nm for peptide **2**. Conformational clustering was performed using the approach of Daura et al.[40] on the set of peptide structures taken at 10 ps intervals from the complete 200 ns trajectories of the simulations. The RMSD values described above were also used as the cutoffs for the conformational clustering. Only the clusters that make up 95% of a trajectory were selected and counted as a function of time.[41] Hydrogen bonds were defined by a maximum hydrogen−acceptor distance of 0.25 nm and a minimum donor−hydrogen−acceptor angle of 135°. Only hydrogen bonds with a population larger than 5% are reported. Distributions of the size of the solute dipole moment calculated using all atoms or the backbone atoms of the peptides are reported. Since the dipole moment of a set of atoms carrying a nonzero total charge depends on the position of the origin, the center of geometry of the solute was used as such.

Folding kinetics were studied by calculating the total residence time and mean residence time in the folded conformation C_F and the number of time periods for which the solute remains folded. The folding free enthalpy was calculated as

$$\Delta G_{\text{folding}} = -k_B T \ln(P_{C_F}/P_{C_U}) \quad (1)$$

where k_B is the Boltzmann constant, T is the temperature, and P_{C_F} and P_{C_U} are the relative probabilities of the system in the folded and unfolded conformational states, respectively. P_{C_F} and P_{C_U} are obtained by counting the relative number of folded and unfolded structures respectively in a trajectory. The total residence time is the product of P_{C_F} and the total simulation time, and the mean residence time is the total residence time divided by the number of folded periods. The number of folded periods was calculated using structures taken at 10 ps intervals from the simulations. If the peptide changed from one conformation to the other and stayed there for at least 20 ps, it was considered a transition between a folded period and an unfolded period.

Interproton distances extracted from the NOE intensities measured in the NMR experiments were compared with the average interproton distances in the simulations calculated using $\langle r^{-6}\rangle^{-1/6}$, where r is the instantaneous interproton distance. The hydrogen−hydrogen distances involving aliphatic hydrogen atoms were calculated by defining virtual (CH_1), prochiral (stereospecific CH_2), and pseudo- (CH_3 and nonstereospecific CH_2) atomic positions, and pseudoatom corrections were added to the distance bounds for the latter, 0.1 nm for nonstereospecific CH_2, 0.15 nm for CH_3, and 0.29 nm for nonstereospecific rotating methyls.[42] ^3J-coupling constants were calculated using the Karplus relation,[43]

$$^3J(H,H) = a\cos^2\theta + b\cos\theta + c \quad (2)$$

where a = 6.4 Hz, b = −1.4 Hz, and c = 1.9 Hz for the calculation of $^3J_{H_N,H_C}$,[44] and a = 9.5 Hz, b = −1.6 Hz, and c = 1.8 Hz for the calculation of $^3J_{H_C,H_C}$.[45]

Table 3. Folding Dynamics and Thermodynamics of Peptides 1 and 2

simulation	$\mathbf{1}_{45A3}$	$\mathbf{1}_{53A6}$	$\mathbf{1}_{54A7}$	$\mathbf{2}_{45A3}$	$\mathbf{2}_{53A6}$	$\mathbf{2}_{54A7}$
number of folded periods	184	129	205	104	200	363
total residence time [ns]	125	157	174	10	23	37
mean residence time [ps]	680	1218	849	96	115	102
fraction folded [%]	63	79	87	5	12	19
free enthalpy of folding [kJ mol^{-1}]	−1.5	−3.7	−5.4	8.3	5.8	4.2

Table 4. Intramolecular Hydrogen Bond Populations of Peptide 1 (in %)

donor···acceptor	$\mathbf{1}_{45A3}$	$\mathbf{1}_{53A6}$	$\mathbf{1}_{54A7}$
NH(1)···O(3)	20	22	16
NH(2)···O(4)	57	77	87
NH(3)···O(5)	60	80	90
NH(4)···O(6)	57	73	74
NH(5)···O(7)	15	24	27

3. RESULTS

3.1. Peptide 1. The atom-positional RMSD of the backbone atoms of residues 2 to 6 with respect to the 3_{14}-helical structure are shown in Figure 2 for MD simulations of peptide **1** as a function of the simulation time together with their distributions. The results show that the folding equilibrium of peptide **1** varies between the different force fields. Although the distributions of RMSD have the same pattern and the location of the major peak

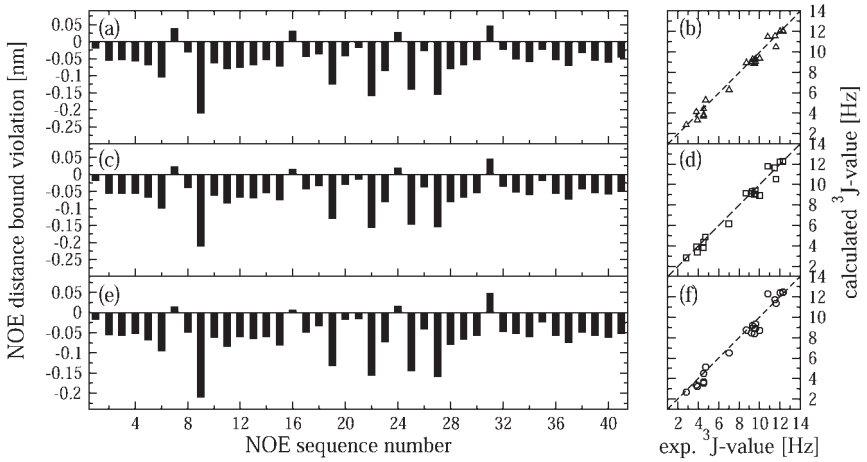

Figure 3. Comparison of $\langle r^{-6}\rangle^{-1/6}$ averaged NOE distance bound violations (left panels) and average ^3J-coupling constants (right panels) as obtained from simulations and experimental data[30] of peptide **1**. Upper panels, $\mathbf{1}_{45A3}$; middle panels, $\mathbf{1}_{53A6}$; lower panels, $\mathbf{1}_{54A7}$. For the specification of the NOE atom pairs and the ^3J-coupling constants, we refer to Tables S1 and S2 in ref 34.

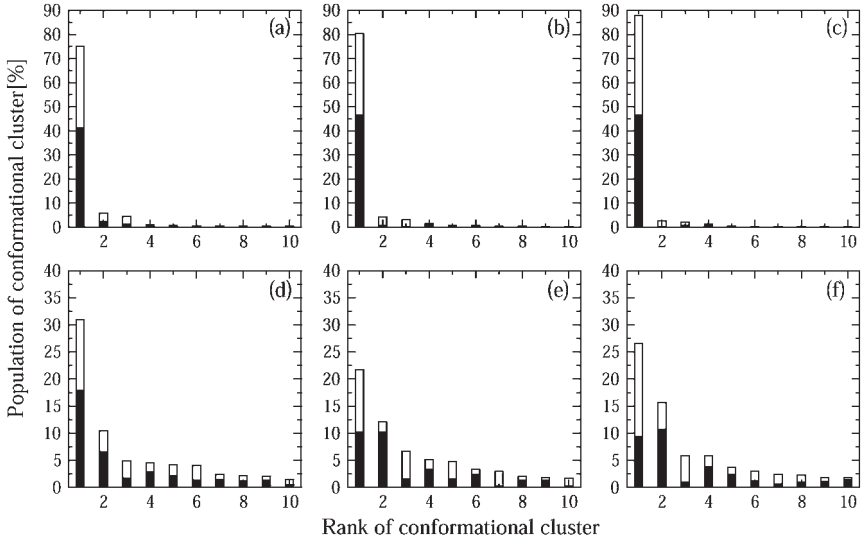

Figure 4. Conformational clustering analysis of the combined trajectories of three force fields for peptide **1** (panels a−c) and peptide **2** (panels d−f). The population in percentage per cluster and the portion of structures per cluster that belong to the trajectories generated using each of the three force fields is shown in decreasing order. (a) $\mathbf{1}_{45A3}$ (white)−$\mathbf{1}_{53A6}$ (black); (b) $\mathbf{1}_{45A3}$ (white)−$\mathbf{1}_{54A7}$ (black); (c) $\mathbf{1}_{53A6}$ (white)−$\mathbf{1}_{54A7}$ (black); (d) $\mathbf{2}_{45A3}$ (white)−$\mathbf{2}_{53A6}$ (black); (e) $\mathbf{2}_{45A3}$ (white)−$\mathbf{2}_{54A7}$ (black); (f) $\mathbf{2}_{53A6}$ (white)−$\mathbf{2}_{54A7}$ (black).

in the distributions is below 0.1 nm in all three simulations, the simulation using the force field 54A7 samples less unfolded conformations than the simulations using the force fields 53A6 and 45A3, see Table 3.

Populations of intramolecular hydrogen bonds in the simulations of peptide **1** are listed in Table 4. The populations of the 3_{14}-helical hydrogen bonds, i.e., those between NH(i) and O(i+2), increase from $\mathbf{1}_{45A3}$ to $\mathbf{1}_{53A6}$ to $\mathbf{1}_{54A7}$, except for the one between NH(1) and O(3), including the terminal residue. The free enthalpy of folding also shows an increased stability of the 3_{14}-helical fold for the successive force fields (Table 3).

Kinetic properties are listed in Table 3. The mean residence time for $\mathbf{1}_{54A7}$ is shorter than that for $\mathbf{1}_{53A6}$ due to the higher frequency of folding events during the former simulation.

The proton−proton NOE distance bound violations and ^3J-coupling constants calculated from the simulations of peptide **1** with the three different force fields are shown in Figure 3. There are four slightly positive violations for the same NOEs in all three simulations. Three of the four positive violations of $\mathbf{1}_{54A7}$ are smaller than those of $\mathbf{1}_{53A6}$ and $\mathbf{1}_{45A3}$. The average ^3J-coupling constants also agree well with the experimental data, with average absolute deviations of 0.4, 0.4, and 0.5 Hz for $\mathbf{1}_{45A3}$, $\mathbf{1}_{53A6}$, and $\mathbf{1}_{54A7}$, respectively, well within the accuracy of the Karplus relation.

To investigate whether the simulations using the different force fields sample the same conformational space, we performed a conformational clustering analysis on combined trajectories of simulations of the same peptide using different force fields. The results are shown in Figure 4. The populations of the clusters in panels a−c show that the conformational spaces sampled in simulations using the three different force fields are not very different.

The cumulative number of conformational clusters that make up 95% of the trajectory in the simulations as a function of time is

shown in Figure 5. All of the numbers of clusters converge within 200 ns, indicating that the simulations converged to a particular set of conformations. Only two clusters comprise 95% of the trajectory in the simulation $\mathbf{1}_{54A7}$. A total of 93% of the trajectory of $\mathbf{1}_{54A7}$ is concentrated in the first cluster. These data also indicate that peptide **1** is more stable with the 54A7 force field than with the 53A6 or 45A3 force fields.

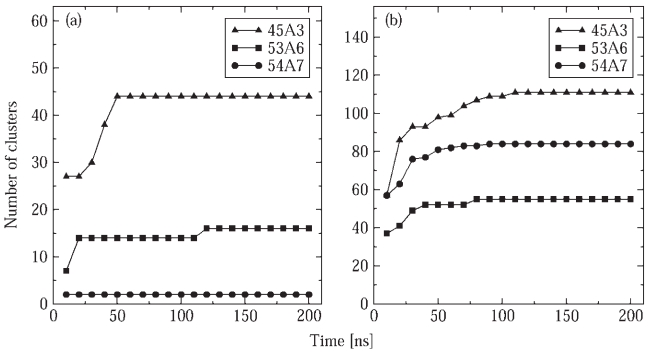

Figure 5. Cumulative number of conformational clusters that make up 95% of the trajectory in the simulations as a function of time. (a) Peptide **1**. (b) Peptide **2**. Triangles, force field 45A3; squares, force field 53A6; circles, force field 54A7.

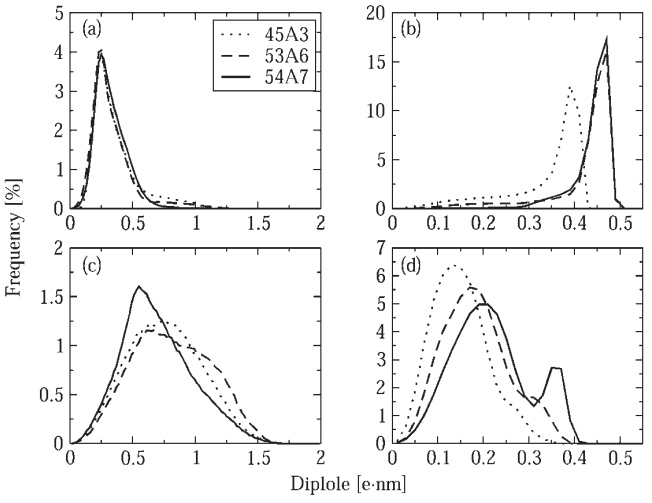

Figure 6. Distributions of solute dipole moment of peptide **1** (upper panels) and peptide **2** (lower panels) calculated using all atoms (left panels) or only the backbone atoms (right panels). Dotted lines, force field 45A3; dashed lines, force field 53A6; solid lines, force field 54A7.

Distributions of the solute dipole moment of peptide **1** are shown in Figure 6. The dipole moment distributions of backbone atoms are different between simulations $\mathbf{1}_{45A3}$ and $\mathbf{1}_{53A6}$ or $\mathbf{1}_{54A7}$, which is due to the larger backbone atomic partial charges in the latter two force fields.[11] Interestingly, the distributions of the dipole moment of the whole peptide, i.e., including the terminal NH_3^+ and COOH groups,[46] are similar.

3.2. Peptide 2. The atom-positional RMSD of the backbone atoms of residues 2 to 5 with respect to the model hairpin structure (X-PLOR structure number 1[33]) are shown in Figure 7 for the simulations of peptide **2** as a function of simulation time together with their distributions. The location of the peak of the distribution is around 0.08 nm in simulation $\mathbf{2}_{54A7}$, while the ones for the other two simulations are both around 0.15 nm. This indicates that the new force field 54A7 samples more ideal hairpin conformations for peptide **2** than the force fields 45A3 and 53A6. Both the total residence time and the fraction of folded conformation gradually increase from $\mathbf{2}_{45A3}$ to $\mathbf{2}_{53A6}$ to $\mathbf{2}_{54A7}$, see Table 3. Thus, the free enthalpy of folding gradually decreases in this order. It indicates that the new 54A7 force field stabilizes the folded hairpin structure over the other two force fields.

Populations of intramolecular hydrogen bonds in the simulations of peptide **2** are listed in Table 5. The populations of the hairpin hydrogen bonds NH(2)···O(5) and NH(3)···O(4) are larger for $\mathbf{2}_{54A7}$ than for $\mathbf{2}_{45A3}$, while being similar to those in $\mathbf{2}_{53A6}$. The sum of the two populations is 50.2% in $\mathbf{2}_{54A7}$ and is 52.8% in $\mathbf{2}_{53A6}$.

Table 5. Intramolecular Hydrogen Bond Populations of Peptide 2 (in %)

donor···acceptor	$\mathbf{2}_{45A3}$	$\mathbf{2}_{53A6}$	$\mathbf{2}_{54A7}$
NH(2)···O(5)	1.8	5.1	11.6
NH(3)···O(4)	30.0	47.6	38.6
NH(4)···O(1)	7.6	16.1	5.5
NH(5)···O(3)	3.5	2.7	7.0
NH(5)···O(6)	5.0	0.1	1.8

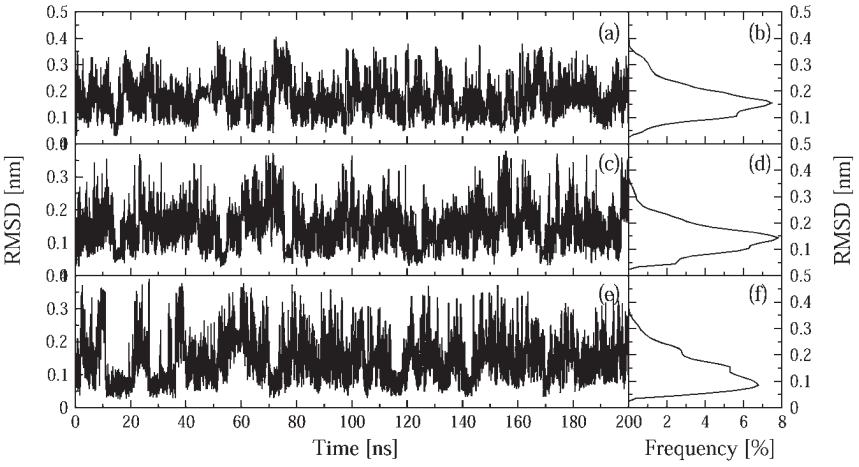

Figure 7. Time evolution (left panels) and distribution (right panels) of the atom-positional RMSD from the model hairpin structure for the backbone atoms of residues 2−5 in simulations of peptide **2**. Upper panels, $\mathbf{2}_{45A3}$; middle panels, $\mathbf{2}_{53A6}$; lower panels, $\mathbf{2}_{54A7}$.

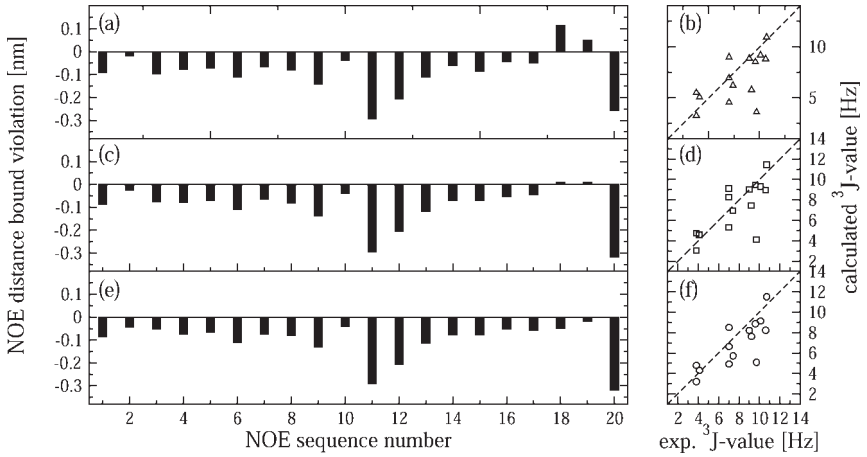

Figure 8. Comparison of $\langle r^{-6}\rangle^{-1/6}$ averaged NOE distance bound violations (left panels) and average ^3J-coupling constants (right panels) as obtained from simulations and experimental data[33] of peptide **2**. Upper panels, $\mathbf{2}_{45A3}$; middle panels, $\mathbf{2}_{53A6}$; lower panels, $\mathbf{2}_{54A7}$. For the specification of the NOE atom pairs and the ^3J-coupling constants, we refer to Tables S4 and S5 in ref 34.

Kinetic properties are listed in Table 3. The mean residence times do not differ much between the three force fields.

The proton−proton NOE distance bound violations and ^3J-coupling constants calculated from the simulations of peptide **2** are shown in Figure 8. There are two positive violations in $\mathbf{2}_{45A3}$, 0.11 and 0.05 nm. Both of these violations are reduced to 0.01 nm in $\mathbf{2}_{53A6}$ and disappear in $\mathbf{2}_{54A7}$. The average absolute deviations of ^3J-coupling constants are 1.6, 1.3, and 1.4 Hz for $\mathbf{2}_{45A3}$, $\mathbf{2}_{53A6}$, and $\mathbf{2}_{54A7}$, respectively. These deviations from the experimental values are larger than those observed for peptide **1**.

The results of the conformational clustering analyses of combined trajectories are shown in Figure 4. It seems that the conformational spaces sampled are most different between $\mathbf{2}_{45A3}$ and $\mathbf{2}_{53A6}$ on the one hand and $\mathbf{2}_{54A7}$ on the other. This is in line with the deviations from the ideal hairpin structure shown in Figure 7. The RMSDs of the central member structures of the first two clusters from the ideal hairpin structure are 0.10 and 0.07 nm for the combined trajectories of $\mathbf{2}_{45A3}$ and $\mathbf{2}_{54A7}$ and are 0.11 and 0.05 nm for the combined trajectories of $\mathbf{2}_{53A6}$ and $\mathbf{2}_{54A7}$. The central member structures of the first clusters are partly folded, while those of the second clusters are fully folded. This indicates that the new 54A7 force field samples more hairpin conformations than the other two force fields.

The cumulative number of conformational clusters that make up 95% of the trajectory in the simulations as a function of time is shown in Figure 5. The numbers of clusters converge in 200 ns for all simulations. Peptide **2** samples a larger conformational space than peptide **1**.

Distributions of the solute dipole moment of peptide **2** are shown in Figure 6. The dipole moment distributions of the whole peptide are broader than those of peptide **1**. The dipole moment of backbone atoms of peptide **1** is larger than that of peptide **2**, because of the stronger alignment of the NH and CO dipoles in the 3_{14}-helix compared to the hairpin.

4. CONCLUSION

To test the performance of the new GROMOS 54A7 force field, we compared the folding behavior of two β-peptides that show a helical and a hairpin as the dominant fold using three different force fields, GROMOS 45A3, 53A6, and 54A7, respectively. The 54A7 force field samples more 3_{14}-helical or hairpin conformations than the 53A6 or 45A3 force fields, which is due to the slightly enhanced capacity of the backbone NH and CO groups to form hydrogen bonds with each other in the 54A7 parameter set. The agreement with the experimental NOE data was slightly improved by using the 54A7 force field, while the experimental ^3J couplings were reproduced equally well in the simulations of the three different force fields.

Overall, the new 54A7 force field reproduces the folding equilibria equally well or slightly better than the 53A6 and 45A3 force fields. Yet, the distributions of conformations are slightly different for the different force fields as are the folding kinetics. The GROMOS 54A7 force field developed to enhance the stability of α-helical structures in proteins can thus be safely used in simulations of folding equilibria of β-peptides.

AUTHOR INFORMATION

Corresponding Author

*E-mail: wfvgn@igc.phys.chem.ethz.ch.

ACKNOWLEDGMENT

This work was financially supported by the National Center of Competence in Research (NCCR) in Structural Biology and by grant number 200020-121913 of the Swiss National Science Foundation, by grant number 228076 of the European Research Council (ERC), and by grants number IZLCZ2-123884 of the Sino-Swiss Science and Technology Cooperation Program, which is gratefully acknowledged.

REFERENCES

(1) Weiner, P. K.; Kollman, P. A. *J. Comput. Chem.* **1981**, *2*, 287–303.
(2) Cornell, W. D.; Cieplak, P.; Bayly, C. I.; Gould, I. R.; Merz, K. M.; Ferguson, D. M.; Spellmeyer, D. C.; Fox, T.; Caldwell, J. W.; Kollman, P. A. *J. Am. Chem. Soc.* **1995**, *117*, 5179–5197.
(3) Pearlman, D. A.; Case, D. A.; Caldwell, J. W.; Ross, W. S.; Cheatham, T. E.; Debolt, S.; Ferguson, D.; Seibel, G.; Kollman, P. *Comput. Phys. Commun.* **1995**, *91*, 1–41.
(4) Brooks, B. R.; Bruccoleri, R. E.; Olafson, B. D.; States, D. J.; Swaminathan, S.; Karplus, M. *J. Comput. Chem.* **1983**, *4*, 187–217.
(5) MacKerell, A. D.; Wiorkiewiczkuczera, J.; Karplus, M. *J. Am. Chem. Soc.* **1995**, *117*, 11946–11975.

(6) MacKerell, A. D.; Bashford, D.; Bellott, M.; Dunbrack, R. L.; Evanseck, J. D.; Field, M. J.; Fischer, S.; Gao, J.; Guo, H.; Ha, S.; Joseph-McCarthy, D.; Kuchnir, L.; Kuczera, K.; Lau, F. T. K.; Mattos, C.; Michnick, S.; Ngo, T.; Nguyen, D. T.; Prodhom, B.; Reiher, W. E.; Roux, B.; Schlenkrich, M.; Smith, J. C.; Stote, R.; Straub, J.; Watanabe, M.; Wiorkiewicz-Kuczera, J.; Yin, D.; Karplus, M. *J. Phys. Chem. B* **1998**, *102*, 3586–3616.

(7) van Gunsteren, W. F.; Berendsen, H. J. C. *Groningen Molecular Simulation (GROMOS) Library Manual*; Biomos: Groningen, 1987.

(8) van Gunsteren, W. F.; Billeter, S. R.; Eising, A. A.; Hünenberger, P. H.; Krüger, P.; Mark, A. E.; Scott, W. R. P.; Tironi, I. G. *Biomolecular Simulation: The GROMOS96 Manual and User Guide*; Vdf Hochschulverlag AG an der ETH Zürich: Zürich, Switzerland, 1996.

(9) Daura, X.; Mark, A. E.; van Gunsteren, W. F. *J. Comput. Chem.* **1998**, *19*, 535–547.

(10) Schuler, L. D.; Daura, X.; van Gunsteren, W. F. *J. Comput. Chem.* **2001**, *22*, 1205–1218.

(11) Oostenbrink, C.; Villa, A.; Mark, A. E.; van Gunsteren, W. F. *J. Comput. Chem.* **2004**, *25*, 1656–1676.

(12) Jorgensen, W. L.; TiradoRives, J. *J. Am. Chem. Soc.* **1988**, *110*, 1657–1666.

(13) Jorgensen, W. L.; Maxwell, D. S.; TiradoRives, J. *J. Am. Chem. Soc.* **1996**, *118*, 11225–11236.

(14) Walser, R.; Mark, A. E.; van Gunsteren, W. F.; Lauterbach, M.; Wipff, G. *J. Chem. Phys.* **2000**, *112*, 10450–10459.

(15) Geerke, D. P.; Oostenbrink, C.; van der Vegt, N. F. A.; van Gunsteren, W. F. *J. Phys. Chem. B* **2004**, *108*, 1436–1445.

(16) Smith, L. J.; Berendsen, H. J. C.; van Gunsteren, W. F. *J. Phys. Chem. B* **2004**, *108*, 1065–1071.

(17) Fioroni, M.; Burger, K.; Mark, A. E.; Roccatano, D. *J. Phys. Chem. B* **2000**, *104*, 12347–12354.

(18) Schmid, N.; Eichenberger, A.; Choutko, A.; Riniker, S.; Winger, M.; Mark, A. E.; van Gunsteren, W. F. *Eur. Biophys. J.* **2010**in press.

(19) Poger, D.; van Gunsteren, W. F.; Mark, A. E. *J. Comput. Chem.* **2010**, *31*, 1117–1125.

(20) Cubberley, M. S.; Iverson, B. L. *Curr. Opin. Chem. Biol.* **2001**, *5*, 650–653.

(21) Cheng, R. P. *Curr. Opin. Struct. Biol.* **2004**, *14*, 512–520.

(22) Hecht, E.; Huc, I. *Foldamers: structure, properties, and applications*; Wiley-VCH, New York, 2007.

(23) Hintermann, T.; Seebach, D. *Chimia* **1997**, *51*, 244–247.

(24) Seebach, D.; Abele, S.; Schreiber, J. V.; Martinoni, B.; Nussbaum, A. K.; Schild, H.; Schulz, H.; Hennecke, H.; Woessner, R.; Bitsch, F. *Chimia* **1998**, *52*, 734–739.

(25) Seebach, D.; Matthews, J. L. *Chem. Commun.* **1997**, *21*, 2015–2022.

(26) Cheng, R. P.; Gellman, S. H.; DeGrado, W. F. *Chem. Rev.* **2001**, *101*, 3219–3232.

(27) van Gunsteren, W. F.; Bürgi, R.; Peter, C.; Daura, X. *Angew. Chem., Int. Ed.* **2001**, *40*, 351–355.

(28) Daura, X.; Glattli, A.; Gee, P.; Peter, C.; van Gunsteren, W. F. *Adv. Protein Chem.* **2002**, *62*, 341–360.

(29) van Gunsteren, W. F.; Gattin, Z. In *Simulation of Folding Equilibria in Foldamers: Structure, Properties, and Applications*; Hecht, S., Huc, I., Eds.; Wiley, Weinheim, Germany: 2007, p 173−192.

(30) Seebach, D.; Ciceri, P. E.; Overhand, M.; Jaun, B.; Rigo, D.; Oberer, L.; Hommel, U.; Amstutz, R.; Widmer, H. *Helv. Chim. Acta* **1996**, *79*, 2043–2066.

(31) Daura, X.; van Gunsteren, W. F.; Rigo, D.; Jaun, B.; Seebach, D. *Chem.—Eur. J.* **1997**, *3*, 1410–1417.

(32) Daura, X.; Jaun, B.; Seebach, D.; van Gunsteren, W. F.; Mark, A. E. *J. Mol. Biol.* **1998**, *280*, 925–932.

(33) Daura, X.; Gademann, K.; Schafer, H.; Jaun, B.; Seebach, D.; van Gunsteren, W. F. *J. Am. Chem. Soc.* **2001**, *123*, 2393–2404.

(34) Lin, Z. X.; Schmid, N.; van Gunsteren, W. F. *Mol. Phys.* **2011**, *109*, 493–506.

(35) Christen, M.; Hünenberger, P. H.; Bakowies, D.; Baron, R.; Bürgi, R.; Geerke, D. P.; Heinz, T. N.; Kästenholz, M. A.; Kräutler, V.; Oostenbrink, C.; Peter, C.; Trzesniak, D.; van Gunsteren, W. F. *J. Comput. Chem.* **2005**, *26*, 1719–1751.

(36) Lin, Z. X.; van Gunsteren, W. F. *Phys. Chem. Chem. Phys.* **2010**, *12*, 15442–15447.

(37) Berendsen, H. J. C.; Postma, J. P. M.; van Gunsteren, W. F.; Dinola, A.; Haak, J. R. *J. Chem. Phys.* **1984**, *81*, 3684–3690.

(38) Ryckaert, J. P.; Ciccotti, G.; Berendsen, H. J. C. *J. Comput. phys.* **1977**, *23*, 327–341.

(39) Tironi, I. G.; Sperb, R.; Smith, P. E.; van Gunsteren, W. F. *J. Chem. Phys.* **1995**, *102*, 5451–5459.

(40) Daura, X.; van Gunsteren, W. F.; Mark, A. E. *Proteins: Struct. Funct. Genet.* **1999**, *34*, 269–280.

(41) Wang, D.; Jaun, B.; van Gunsteren, W. F. *ChemBioChem* **2009**, *10*, 2032–41.

(42) Wüthrich, K.; Billeter, M.; Braun, W. *J. Mol. Biol.* **1983**, *169*, 949–961.

(43) Karplus, M. *J. Chem. Phys.* **1959**, *30*, 11–15.

(44) Pardi, A.; Billeter, M.; Wüthrich, K. *J. Mol. Biol.* **1984**, *180*, 741–751.

(45) de Marco, A.; Llinas, M.; Wüthrich, K. *Biopolymers* **1978**, *17*, 617–636.

(46) Gee, P. J.; van Gunsteren, W. F. *Proteins Struct. Funct. Bioinf.* **2006**, *63*, 136–143.